IEEE Access
Multidisciplinary | Rapid Review | Open Access Journal

Received September 1, 2018, accepted September 22, 2018, date of publication October 1, 2018, date of current version October 29, 2018.

Digital Object Identifier 10.1109/ACCESS.2018.2873348

Exploring the Capability of Compact Polarimetry (Hybrid Pol) C Band RISAT-1 Data for Land Cover Classification

KIRAN DASARI, (Student Member, IEEE), AND ANJANEYULU LOKAM, (Member, IEEE)
Department of Electronics and Communication Engineering, National Institute of Technology, Warangal 506004, India

Corresponding author: Kiran Dasari (kirandasari16@gmail.com)

The datasets used in this study have been procured with the financial support of National Institute of Technology, Warangal, India.

ABSTRACT Compact Polarimetry has gained significant importance in recent years among other earth observation missions due to its low power consumption, simple architecture, and larger swath width. For space-based SAR systems, these parameters are vital to monitor the earth surface continuously for various applications. The main manifestations of Hybrid polarimetry from fully polarimetric systems is transmitting a circular polarization and receiving in linear polarizations. In this paper, we assess the performance of compact polarimetry (hybrid polarimetry) over dual-pol RISAT-1 data for land cover classification over various ground targets using backscattered coefficient values, degree of polarization, and relative phase values. In order to understand the scattering mechanism of the targets, Raney decomposition, Pseudo Three Component decomposition, m-δ and m-χ decompositions were performed on the SAR datasets. The m-χ decomposition has proven to be robust when transmitting component is not perfectly circularly polarized. The support vector machine (SVM) classifier algorithm was used to classify the datasets. Three datasets (viz. RISAT-1 hybrid-pol data, RISAT-1 dual-pol data, and Resourcesat-2 data) were evaluated with SVM classifier and compared using three different kernel parameters, i.e. radial basis function (RBF), Polynomial with degree '2' and Linear. From this paper, it was observed that the SVM with RBF kernel parameter gave highest Overall Accuracy (OA) of 92.34% for hybrid Pol RISAT-1 data. Similarly, the SVM with RBF kernel parameter gave an overall accuracy (OA) of 76.83% for dual-pol RISAT-1 data. SVM has classified the datasets into four classes viz. Urban, Water, Vegetation, and Bare soil. The evaluation of classified datasets were performed using confusion matrix for accuracy assessment. For validating the results, the classified image is compared with the optical imagery of Resourcesat-2 (LISS IV) sensor, Google Earth, and In-situ information that was collected synchronous to the satellite pass on July 5, 2016.

INDEX TERMS Compact polarimetry, m-delta, m-chi decomposition, hybrid polarimetry, land cover classification, RISAT-1, SVM classifier.

I. INTRODUCTION

Indian Space Research Organization (ISRO) has launched many Earth-Observing (EO) satellites, since 1979, beginning with Bhaskara - I, as it was the first experimental remote sensing satellite built by ISRO [1]. Indian Remote Sensing Satellite (IRS-1A) was the first series of indigenous remote sensing satellite launched into the orbit on March 15, 1988. As on today, ISRO has launched 30 (27 optical and 3 Radar) Earth Observation missions and also has the largest constellation of remote sensing satellites in operation [2]–[4]. Earth-observing satellites are mainly used for remote sensing purpose to monitor the Earth constantly. Satellites with optical sensors were providing the data from past three decades. Moreover, optical sensors may not support in all weather conditions and night acquisition is not possible. Therefore, remote sensing using microwaves came into existence to overcome the limitations of optical remote sensing. Radar Imaging Satellite (RISAT-2) was the first microwave (SAR) based remote sensing satellite launched on April 20, 2009; which was built by IAI/MBT (Israel Aerospace Industries Ltd.) and operates in X-band. RISAT-2 was a prelude to RISAT-1 [5]. ISRO launched Radar Imaging Satellite (RISAT-1) on April 26, 2012. RISAT-1 was the first indigenous SAR based Space-borne mission from ISRO and was also the first (EO) space-borne mission with Hybrid polarimetry [6]. Mini SAR (Mini Synthetic Aperture) on Chandraayan-1 mission and Mini-RF (Miniature Radio Frequency) instrument on Lunar Reconnaissance Orbiter

mission were launched in 2008 and 2009 respectively. These two missions were aimed for lunar and planetary studies with hybrid polarimetry outside the earth orbit [7]–[8]. The unique characteristics of C-band SAR with Hybrid polarimetry enables wide application in the field of agriculture (Paddy monitoring), ship detection, oil slick monitoring, forestry, geology, soil moisture and in disaster management during the time of flood and cyclone [9].

A. RADAR POLARIMETRY

Radar polarimetry is the science of acquiring, processing and analyzing the polarization state of the electromagnetic field and is concerned for the utility of polarimetry for radar application. With recent advances in polarimetry, many upcoming SAR based space-borne missions are planned to overcome the trade-off such as polarimetry, resolution and swath width. From past two decades, the concept polarimetric SAR and its application have been an active field of research. Radar polarimetry can be performed on two platforms, i.e., Space-borne and Airborne SAR systems by providing high-resolution data in single, dual and quad-pol data for the radar community. In general, a single pol system transmits and receives only one polarization viz. horizontal (H) or vertical (V). Similarly, a dual-pol SAR transmits one polarization and receives the backscatter in a pair of orthogonal polarization viz. transmit (H) and receives (H, V) vice versa. In quad-pol SAR, two orthogonal polarizations H and V are coherently transmitted and received. From quad-pol SAR, complete polarimetric scattering information can be obtained from the target, and hence better analysis and classification can be performed [10].

B. COMPACT POLARIMETRY OVERVIEW

The functionality of fully quad-pol SAR systems is illustrated in the Fig. 1. It shows the timing sequence of transmitted and received signal for a quad-pol SAR. A pulse is first transmitted on one polarization, and all orthogonally polarized signals are received before the next signal is transmitted. Similarly,

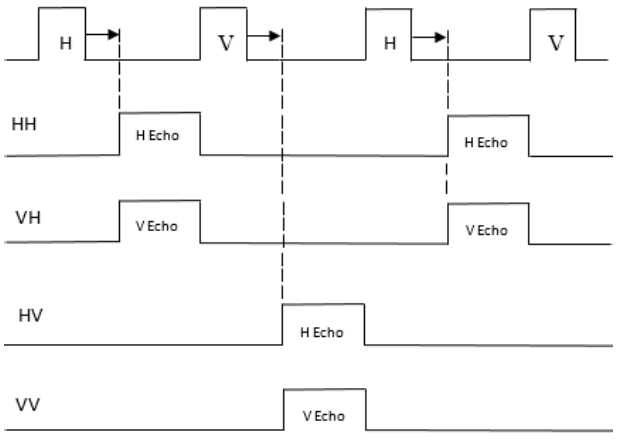

FIGURE 1. Sequence of transmitted and received echo signal in fully polarimetric systems.

SAR transmits two orthogonal polarized pulses alternatively and receives backscattered signal simultaneously using two orthogonally polarized antenna thus by capturing all polarization information. This process doubles, pulse repletion frequency (PRF) and halves the swath width which is the limitation to the fully quad-pol SAR systems. These limitations will have an adverse effect on the revisit time, which is an important factor for earth observation missions [11]. The trade off's between conventional single-pol linear systems and quad-pol systems is a dual-pol system, in which a single polarization is transmitted and receives two orthogonal polarizations, by overcoming the drawbacks of conventional linear polarization systems. To achieve better swath width and to reduce average peak power with simple architecture Compact polarimetry (Dual Partial Polarimetric mode) has been proposed [12]. The dual partial polarimetric mode was proposed by Souyris and Mingot [13]. The information from the compact-pol SAR is almost similar to that of fully polarimetric SAR from the azimuthally symmetric scattering targets and was proved by Souyris and Mingot [13]. Nord *et al.* [14] drew a similar conclusion and also promoted the use of Hybrid SAR for its simpler architecture in contrast to the conventional SAR. Compact polarimetry is a technique which allows construction of pseudo quad-pol data from dual-pol SAR. Recently Compact polarimetry has gained more importance than fully polarimetric SAR by its advantages such as larger swath width, less power,and simple architecture. Compact polarimetry has proven its potential in distinguishing oil slicks, ship detection and in crop monitoring. Compact polarimetry has three modes as shown in Table 1 and Fig. 2.

TABLE 1. Compact polarimetry modes.

S.No.	Mode	Tx/Rx(Transmission/Reception)
1	$\pi/4$	45°/(H,V)
2	CTLR (Hybrid)	RC/(H,V)
3	DCP	RC/(RC,LC)

H = Horizontal, V = Vertical, RC = Right Circular, LC = Left Circular, S.No = Serial Number

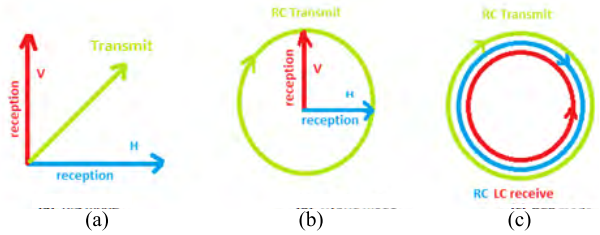

FIGURE 2. Illustration of three modes of Compact Polarimetry.

1) ($\pi/4$) MODE

The ($\pi/4$) mode was one of the first partial polarimetric concepts to appear in the radar imaging literature developed by Souyris and Mingot [13]. In this mode, SAR transmits

a linear polarized field at an angle of 45° concerning Horizontal or vertical orientation and receives Horizontal and vertical components [12], [13]. The covariance matrix is obtained from the Eqn. 1, as shown at the bottom of this page.

2) DUAL CIRCULAR POLARIMETRIC (DCP)

In this mode, right circular polarization is transmitted and both left and right circular polarization are received. Stacy and Preiss [14] demonstrated that dual circular polarization could be implemented with slight modification from original compact polarimetry algorithm. The covariance matrix was obtained from the Eqn. 2, as shown at the bottom of this page.

3) CIRCULAR TRANSMIT LINEAR RECEIVE (CTLR) POLARIMETRY

CTLR is popularly known as Hybrid polarimetry. In Hybrid polarimetry, only one polarization will be transmitted, and other orthogonal polarization will be received along with relative phase which is different from dual polarimetry systems. In this mode, Circular (right or left) component is Transmitted and Linear component is Received (CTLR). In dual polarimetry systems, relative phase information is not available. Hybrid Polarimetry is the optimum architecture for applications related to planetary explorations and earth observations. SAR systems transmitting linear component may not be able to excite target response from linear structures as they are orthogonally oriented to the incident electric field. Quad-pol SAR system is restricted in terms of incidence angle. In this case, by transmitting a linear component volume scattering is overestimated due to the change in orientation angle shift during reception of the signal from the target. Therefore illuminating circularly polarized signal can overcome the limitation of linear transmitted systems. However, transmitting a circular component will not be affected by ionospheric distortions (Faraday rotation) and are free from the polarization orientation angle shift [11]. Hence, overestimation of volume scattering can be reduced

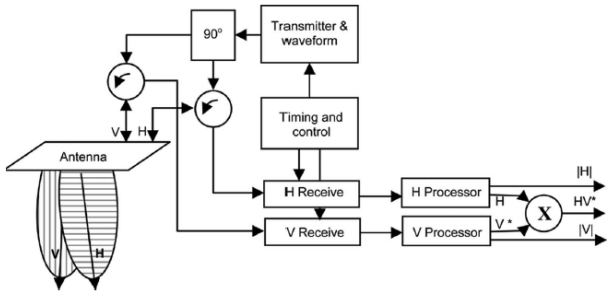

FIGURE 3. Hybrid polarimetry Architecture.

when compared to quad-pol SAR system and another advantage of transmitting circular polarization is to reduce the range ambiguities [15]. Among circular transmit systems, Hybrid-pol is preferred over DCP because its performance is limited to weaker cross-polarized links and it is affected by additive noise and by crosstalk from stronger like polarized signal [11]. From hybrid-pol data, an equivalent covariance or coherency matrix may be reconstructed to produce pseudo-quad-pol data. From the Eqn. 3, as shown at the bottom of this page, covariance matrix of hybrid-pol data was obtained.

4) HYBRID POLARIMETRY SAR ARCHITECTURE

Hybrid Polarimetry architecture is shown in Fig. 3. The hardware realization of hybrid polarimetry is in-complex as compared to that of linear full polarimetric systems. Both in active and passive case, the dual polarized antenna will transmit circular polarization only if H and V components are driven simultaneously. In this system, the same signal is transmitted through horizontal and vertical antenna such that phase 90° is maintained. Simultaneously during the reception, an additional pair of 90° hybrids in the receive paths is required after the antenna or along each of receive chains. Hybrid polarimetry architecture has numerous advantages such as the generation of Stokes parameter from dual-pol data, less risk of crosstalk, calibration, less flight hardware, quad polarization transformation [16].

$$[C_{\pi/4}] = \frac{1}{2}\begin{bmatrix} |S_{HH}|^2 & (S_{HH}.S_{VV}^*) \\ (S_{HH}^*.S_{VV}) & |S_{VV}|^2 \end{bmatrix} + \frac{1}{2}\begin{bmatrix} |S_{HV}|^2 & |S_{HV}|^2 \\ |S_{HV}|^2 & |S_{HV}|^2 \end{bmatrix} + \frac{1}{2}\begin{bmatrix} 2\Re(S_{HH}.S_{HV}^*) & S_{HH}.S_{HV}^* + S_{VV}^*.S_{HV} \\ S_{HH}^*.S_{HV} + S_{VV}.S_{HV}^* & 2\Re(S_{VV}.S_{HV}^*) \end{bmatrix} \tag{1}$$

$$[C_{DCP}] = \frac{1}{4}\begin{bmatrix} |S_{HH} - S_{VV}|^2 & -i(S_{HH} - S_{VV}) \\ i(S_{HH} + S_{VV}).(S_{HH} - S_{VV})^* & |(S_{HH} + S_{VV})|^2 \end{bmatrix} + \frac{1}{4}\begin{bmatrix} 4|S_{HV}|^2 & 0 \\ 0 & 0 \end{bmatrix} + \frac{1}{4}\begin{bmatrix} 4\Im((S_{HH} - S_{VV}).S_{HV}^*) & 2(S_{HH} + S_{VV})^*.S_{HV} \\ 2(S_{HH} + S_{VV}).S_{HV}^* & 0 \end{bmatrix} \tag{2}$$

$$[C_{CTLR}] = \frac{1}{2}\begin{bmatrix} |S_{HH}|^2 & i(S_{HH}.S_{VV}^*) \\ -i(S_{HH}.S_{VV}^*) & |S_{VV}|^2 \end{bmatrix} + \frac{1}{2}\begin{bmatrix} |S_{HV}|^2 & -i|S_{HV}|^2 \\ i|S_{HV}|^2 & |S_{HV}|^2 \end{bmatrix} + \frac{1}{2}\begin{bmatrix} -2\Im(S_{HH}.S_{HV}^*) & S_{HH}.S_{HV}^* + S_{VV}^*.S_{HV} \\ S_{HH}^*.S_{HV} + S_{VV}.S_{HV}^* & 2\Im(S_{VV}.S_{HV}^*) \end{bmatrix} \tag{3}$$

II. DATASETS AND STUDY AREA

A. DATASETS

In this study, we have procured two RISAT-1 (Hybrid Pol and Dual pol data) and one Optical Resourcesat-2 data from the National Remote Sensing Center (NRSC), Hyderabad, INDIA as shown in Table 2.

RISAT-1 was launched on 26th April 2012 by ISRO. RISAT-1 is operated in 4 modes, viz. High-Resolution Spotlight (HRS), Fine Resolution Stripmap (FRS-1, FRS-2), Medium Resolution ScanSAR (MRS), Course Resolution ScanSAR (CRS) mode as shown in Table 3. RISAT-1 products are available in four levels: i) level '0' raw data, ii) level 1 ground range geo-tagged SLC data and, iii) level 2 is Terrain corrected Geo-referenced data, iv) level 2A is an enhanced Terrain corrected Geo-referenced data. The data acquired at an altitude of 543.9 km with an incidence angle of 39.5° for hybrid-pol data and an altitude of 544.4 km with an incidence angle of 46.5° for dual-pol data in left look direction. FRS-1 mode with 25 km swath width and 3-meter resolution were opted for this study in ascending mode [17].

TABLE 2. Data sets.

S.No.	Mission/ Sensor	IM	DoA	Polarization	Resolution (m)
1	RISAT-1	FRS-1	5 July 2016	CTLR (Hybrid)	3
2	RISAT-1	FRS-1	5 December 2015	Dual-Pol	3
3	Resourcesat-2/ LISS IV	-	9 April 2016	B2 Visible B3 Infrared 3r4g2b	5.8
4	Google Earth	-	-	-	-

IM = Imaging modes; DoA = Date of Acquisition; S. No. = Serial number;

TABLE 3. Imaging modes of RISAT-1.

S.No.	IM	Swath (Km)	Slant Range Resolution(m)	Polarization
1	HRS	10	1	Single/Dual/Circular
2	FRS-1	25	3	Single/Dual/Circular
3	FRS-2	25	6/9	Quad/Circular
4	MRS	115	25	Single/Dual/Circular
5	CRS	223	50	Single/Dual/Circular

Resourcesat-2 was the 18th Remote Sensing satellite built by ISRO. Resourcesat-2 was launched on April 20, 2011, which was a successor mission of Resourcesat-1. Resourcesat-2 carries three electro-optical cameras as its payload viz. LISS-3, LISS-4, and AWIFS. LISS -4 is a high-resolution multi-spectral camera with a 5.8-meter spatial resolution [18].

B. STUDY AREA

The study area is located in the northern part of Telangana State in the Ghanpur Village, district of Warangal, INDIA. The Geo-coordinates of the study area Lat. 17°69′7.96″N and Long. 79°32′25.6″E. The study area has a complex terrain with mango gardens, paddy fields, cotton fields, waterbodies, and hills.

C. GROUND TRUTH

Ground truth data was collected on 4th and 5th of July 2016. Detailed information such as water level, crop yield progress, weather conditions were also recorded. On 4th and 5th, July the study area was covered with clouds and had rainfall, during the time of acquisition. For better classification accuracy, ground coordinates for various target class were recorded with the help of hand-held GPS of Trimble Company. With the help of ground coordinates, training sites are given for supervised classification. Based on the ground truth, we have identified four classes (Urban, Water Body, Vegetation, Bare Soil).

III. METHODOLOGY

A. IMPORTING DATA

The hybrid-pol and dual-pol datasets of RISAT-1 and Resourcesat-2 are imported into the respective processing tools. Input RISAT-1 data format consists of Dual Polarization elements. The approach is shown in Fig. 4.

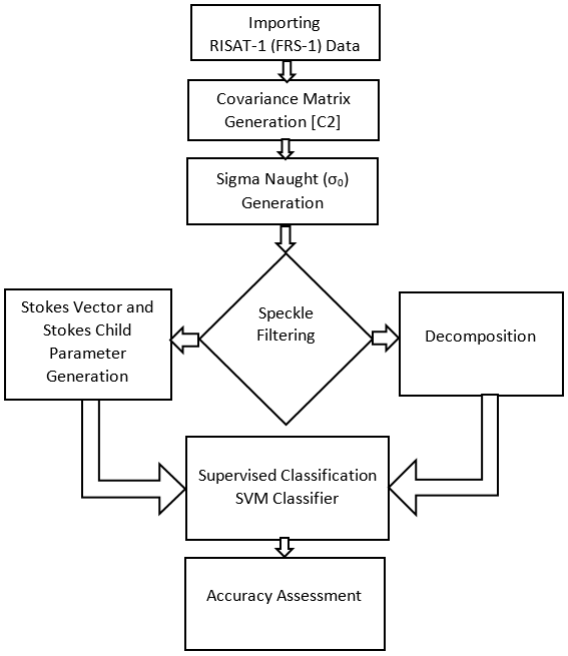

FIGURE 4. Flowchart for the proposed work.

B. DATA PREPROCESSING

The data pre-processing can be performed in two parts. The first approach is to generate backscattering coefficient value for the data; the second approach is polarimetric data processing. In both approaches [C2] matrix generation and speckle filter is a common procedure. The first approach is to generate sigma naught values, then the data has to be multi-looked (2x2) looks in range and azimuth direction and has to undergo speckle filtering to reduce the speckle in the data. In this study, refined lee filter with 7x7 window size

was opted. Later, radiometric calibration was carried out for the generation of sigma naught using the Eqn. 4.

$$\sigma^{\circ}(dB) = 20log_{10}(DN_p) - K_{dB} + 10log_{10}\left(\frac{Sin(i_p)}{Sin(i_{centre})}\right) \tag{4}$$

Where σ_0 is the radar backscattering coefficient, DN_p is the digital number, K_{dB} is the calibration constant, i_p is the incidence angle for pixel position and i_c is the incidence angle at the Centre. The Calibration constant for RV channel is 67.400 and for RH channel is 70.319.

In polarimetric processing, the data is multi-looked and extracted into covariance matrix [C2]. As the SAR data consists of speckle, refined lee filter with 7x7 was opted to remove speckle. Stokes vector and stokes child parameters were derived from the covariance matrix.

C. STOKES PARAMETER GENERATION

When a signal is transmitted on a certain polarization, all the backscattered signal information will be captured in the form of Stokes vector. The set of values which describes the polarization state of the electromagnetic signal is known as Stokes parameter. The four Stokes parameters from the backscattered signal are represented in the form of a matrix as

$$\begin{bmatrix} S_1 \\ S_2 \\ S_3 \\ S_4 \end{bmatrix} = \begin{bmatrix} \langle |E_{RH}|^2 \rangle + \langle |E_{RV}|^2 \rangle \\ \langle |E_{RH}|^2 \rangle - \langle |E_{RV}|^2 \rangle \\ 2\,Re\langle E_{RH}.E_{RV}^* \rangle \\ -2\,Im\langle E_{RH}.E_{RV}^* \rangle \end{bmatrix} \tag{5}$$

From the Eqn. 5, E_{RH} represents voltage received by the channel with right circular transmit and horizontal (linear) receive. Correspondingly E_{RV} represents voltage received by the channel with right circular transmit and vertical receive, and $< \ldots >$ denotes ensemble average. The other way of describing the polarization of the wave in the case of partially polarized waves is with the utility of Stokes parameters. In hybrid polarimetry, to characterize the return signal Stokes parameters are sufficient. From the Stokes vector, child parameters such as the degree of depolarization, the degree of linear and circular polarization ratio are derived [16].

1) THE DEGREE OF POLARIZATION (DoP)

The ratio of power in the polarized part of an electromagnetic wave to the total power in the electromagnetic wave is known as the degree of polarization. DoP refers to the property of the scatterer within a radar resolution cell. DoP values range from 0 to 1. An electromagnetic wave has a polarized and non-polarized component. For a pure scatter the value will be 1 and for a depolarizing scatterer, the value will be 0. The convenient way of expressing the powers in two forms are stokes parameters [19]. While $\sqrt{S_2^2 + S_3^2 + S_4^2}$ gives the total power in the polarized part, the degree of polarization in terms of Stokes parameters can be expressed as

$$D_{pol}(m) = \sqrt{\frac{S_2^2 + S_3^2 + S_4^2}{S_1}} \tag{6}$$

2) RELATIVE PHASE (δ)

Relative Phase is defined as the ratio of the phase difference between the two orthogonal components of the electric vector. The relative phase is most sensitive to polarimetric variation from the backscattered signal from the targets. Under the condition of circularly polarized illumination, δ is the prime indicator of double bounce scatter. The relative phase indicates the type of scattering dominates in a resolution cell, and it ranges between -180 to $+180$. It is evident from Eqn. 7 that δ includes the contribution of S3 and S4.

$$\delta = arc\,tan\left(\frac{S_4}{S_3}\right) \tag{7}$$

3) CIRCULAR POLARIZATION RATIO

Circular Polarization Ratio (CPR) directly relates to the surface roughness, i.e. CPR increases with increase in surface roughness. In case of double-bounce and volume scattering, the CPR value is high due to higher value in the numerator than in the denominator of the CPR and can be expressed in the form as shown in Eqn. 8.

$$\mu_c = \frac{(S_1 - S_4)}{(S_1 + S_4)} \tag{8}$$

D. DECOMPOSITION

The scattering information from the backscatter signal is recorded in the form of scattering matrix. The scattering matrix allows the characterization of the given scatters for a given frequency from the target. In reality, polarimetric SAR data interpretation is very challenging due to complexity of scattering process from various targets. Thus Polarimetric decomposition appears to be a solution in interpreting the information provided by the scattering coherency, and covariance matrices. Decomposition is a broad class of strategies that have proven utility in classifying radar backscatter through the associated covariance matrix. Compact polarimetry has 2x2 covariance matrix and has two methods for decomposition. In the first method, a 3x3 covariance matrix is required for decomposition, but the CP has an only 2x2 matrix. Therefore from a 2x2 covariance matrix, a 3x3 pseudo-quad-pol is generated with certain symmetry assumptions that cannot meet in all situations. The disadvantage of this approach is there is no theoretical justification from 2x2 to 3x3 covariance matrix. In the second method, an alternate decomposition for compact pol data [2x2] data is by using four Stokes vector elements. m-delta (δ) and m-chi (χ) decompositions are examples of the alternate decomposition using Stokes vector elements.

1) RANEY DECOMPOSITION

This decomposition was proposed by Raney. From Raney decomposition, six Raney derived parameters were obtained, i.e. i) Raney odd bounce, ii) Raney double bounce, iii) Raney random, iv) Raney-m, v) Raney-delta, vi) Raney-chi. Raney decomposition utilizes first three parameters to construct a RGB composite image. From these derived parameters along

with first Stokes parameter (S_1), m-delta (δ) and m-chi (χ) decomposition were performed. Whereas m-chi decomposition utilizes 'm' and chi parameters from Raney derived parameters and (S_1) from the first Stokes parameter. Similarly, m-delta decomposition utilizes 'm' and delta parameters from Raney derived parameters.

2) PSEUDO THREE COMPONENT DECOMPOSITION

This decomposition was developed by S. R. Cloude. In [9, eq. (7)], a three- component compact decomposition was proposed, P_V is the volume component, P_S is the surface component and P_D is the dihedral component. Using the geometrical factor single component is split into two components i.e. dihedral and surface component. The split can be represented in the form of decomposition parameters as shown in Eqn. 9. A pseudo three component decomposition using a geometrical factor is shown in Eqn. 10. Where (S_1) is the first stokes vector [20].

$$\tan\delta = \frac{S_4}{S_3} = \frac{cos2\alpha_s}{sin2\alpha_s sin\phi} = \frac{1}{tan2\alpha_s sin\phi} \tag{9}$$

$$\begin{bmatrix} P_D \\ P_V \\ P_S \end{bmatrix} = \begin{bmatrix} \frac{1}{2}S_1 m\,(1 - cos(2\alpha_s)) \\ S_1\,(1-m) \\ \frac{1}{2}S_1 m\,(1 + cos(2\alpha_s)) \end{bmatrix} \tag{10}$$

3) m-DELTA (δ) DECOMPOSITION

m-delta is one of the child parameters derived from Stokes vector and was also found to be an important tool for polarimetric analysis. This technique was proposed and developed by Raney [16] using the principle of relative phase difference between horizontal and vertical polarized backscatter signal. In this technique, total intensity is segmented into polarized and unpolarized using a degree of polarization (m). Polarized part is subdivided into the even bounce and odd bounce by using the relative phase information. The unpolarized part is considered as volume component. In this decomposition, red represents single bounce, green represents volume component, and blue represents the double bounce as shown in Fig. 7(b) and Eqn.11.

$$\begin{aligned} R &= \sqrt{S_1 m \frac{1 - sin\delta}{2}} \\ G &= \sqrt{S_1(1-m)} \\ B &= \sqrt{S_1 m \frac{1 + sin\delta}{2}} \end{aligned} \tag{11}$$

4) m-CHI (χ) DECOMPOSITION

The m-chi decomposition was proposed by Raney [16] and it can be calculated using the Stokes parameters, (S_1) and (S_4), and the degree of polarization 'm' as shown in Eqn. 12. General decomposition techniques which are used for quad-pol data are not applicable to hybrid polarimetric and dual-pol data because compact-pol data and dual-pol data consist of the 2x2 covariance matrix. The degree of polarization' is a natural choice for the first decomposition variable for hybrid dual-pol data. The Poincare ellipticity parameter χ is the best choice for second decomposition variable. m-chi decomposition was tested on lunar orbiter mission, and this method was proven to be an excellent tool for hybrid polarimetric data. In hybrid polarimetry for every scattering, the electric field loses its circularity and hence it is a principle of this technique as shown in Eqn. 13. The unpolarized part is considered as volume component, and polarized part is categorized into odd and even bounce using χ. Blue color indicates single bounce (Bragg scatters), red indicates double bounce and green indicates randomly polarized constitute [21] as shown in Fig. 7(c).

$$Sin(2\chi) = -\frac{S_4}{m} * S_1 \tag{12}$$

m-chi decomposition can be expressed in a color-coded image where

$$\begin{aligned} B &= \sqrt{S_1 m \frac{1 - sin\chi}{2}} \\ G &= \sqrt{S_1(1-m)} \\ R &= \sqrt{S_1 m \frac{1 + sin\chi}{2}} \end{aligned} \tag{13}$$

E. SUPPORT VECTOR MACHINE (SVM) CLASSIFIER

Classification is the task of assigning a given set of data (pixels) to a given class such that the cost of assigning is minimum [22]. The major steps involved in image classification includes feature extraction, selection of training samples and finally classifying the data using suitable classifier. There are two types of classification techniques: parametric and non-parametric. Furthermore, parametric classification can be performed in two approaches, i.e., supervised and unsupervised classification. In unsupervised approach, image is classified automatically by finding the clusters based on certain criterion. In supervised approach, the analyst has to identify location and land cover type using field data (ground truth). Further, the analyst has to locate these areas on the remote sensing data and these areas are known as training sites. In supervised technique, selection of training sets without ground truth data makes the analyst difficult and leads to poor classification. The classification procedure usually involves separating the data into training sets and testing sets. Each instance in the training set contains a class label and several features. The goal of SVM is to produce a model based on training data that can predict target values of the test data.

SVM is a supervised non-parametric classification approach derived from statistical learning theory that often yields good classification results from the complex and noisy data [23]–[26]. As SVM classifier fall under non-parametric classification, estimation of statistical parameters is not involved before classification and therefore they are more appropriate for classifying Remote Sensing data [27]. The advantage of non-parametric approach is that they do not require one specific statistical distribution model, hence they are versatile enough to be implemented in various datasets with minimal training sets. [28]. The main objective of SVM

is to produce a model based on the training sets which can predict target values of the test sets. As SVM classifier is well suited to handle linear non-separable cases using Kernel theory, therefore SVM classifier was used effectively to hyperspectral remote sensing data and on SAR data. [29]

A brief discussion regarding the SVM classifier can be found in [30], [31]. SVM can be performed using either of the three approaches; 1) linear case, 2) Non-linear case 3) Multi-class case. SAR images can be classified in two stages, firstly extraction of appropriate features and secondly labeling the features based on a set of decision rules.

1) LINEAR CASE

Let us consider a two-class classification with N-vectors of training set from 'd'-dimensional feature-space for separating two classes. From the Fig. 5a, two classes (vectors) are represented in red and blue color, the green color line which separates the two classes is called hyperplane [32]. The vectors which are close to the hyperplane are called as support vectors. The distance between support vectors and the hyperplane is called margin. The objective of SVM is to compute optimum hyperplane by maximum margin and by finding minimum $1/(\omega)$. The optimization is performed using Eqn. 15. Each sample is described as $x_i \in \Re^d (i = 1, 2, \cdots N)$ and the target $Y_i \in -1, +1$ is associated with every sample x_i. The optimum hyperplane is defined by

$$\begin{aligned} f(x_i) &= \omega x_i + b \\ sgn[f(x_i)] &= Y_i \\ Y_i(\omega x_i + b) &> 0 \end{aligned} \tag{14}$$

The membership decision rule is based on the function $sgn[f(x_i)]$.

In finding optimum hyperplane, we have to estimate Y_i where $Y_i(\omega x_i + b) > 0$

The optimization is performed using Lagrangian formalism

$$f(x) = \sum_{i=1}^{N} Y_i \alpha_i (x x_i) + b \tag{15}$$

Where α_i denotes Lagrange multiplier. SVM classifies the data into different classes by determining the set of support vectors that summarizes a hyperplane. SVM has a robust feature which ignores the outliners and finds the best hyperplane with maximum margin.

2) NON-LINEAR CASE

From Fig. 5b, two classes (vectors) are represented in red and blue color, the green color line which separates the two classes are called hyperplane. In this case, the first step is to make a soft margin that adapts noisy data. The second step is the utility of kernel. Kernel is a function that simulates the projection of initial data in a feature space with higher dimensions $\phi = K^n \rightarrow H$ as shown in Fig. 5(b). In this new space the data is considered as linearly separable by replacing the dot product $\langle X_i, X_j \rangle$ with $\langle \phi(x), \phi(x_i) \rangle$.

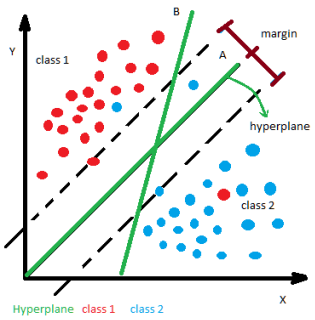

(a)

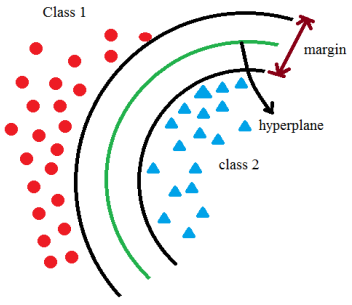

(b)

FIGURE 5. SVM classifier scheme. (a) Linear case. (b) Non-linear case.

The new function to classify the data are

$$f(x) = sign\left(\sum_{i=0}^{N_s} y_i \alpha_i K\left\langle X_i, X_j \right\rangle + b\right) \tag{16}$$

Generally, three kernel are used in this approach i) polynomial kernel, 2) sigmoid kernel, 3) RBF kernel. The polynomial kernel is represented as

$$K(X, X_i) = (\langle X.X_i \rangle + 1)^p \tag{17}$$

The sigmoid kernel is represented as

$$K(X, X_i) = tanh\left(\langle X.X_i \rangle + 1\right) \tag{18}$$

The RBF Kernel is represented as

$$K(X, X_i) = exp^{-\frac{|X - X_i|^2}{2\sigma^2}} \tag{19}$$

3) MULTI CLASS CASE

SVM classifier was designed for binary classification. To handle more than two problems or multi problems there are different algorithms such as One against All (OAA) [29] and One Against One (OAO). OAA algorithm constructs K number of hyperplanes for K classes and separates k and $k-1$ classes. OAO algorithms constructs $\frac{k(k-1)}{2}$ hyperplanes to separate each pair of classes.

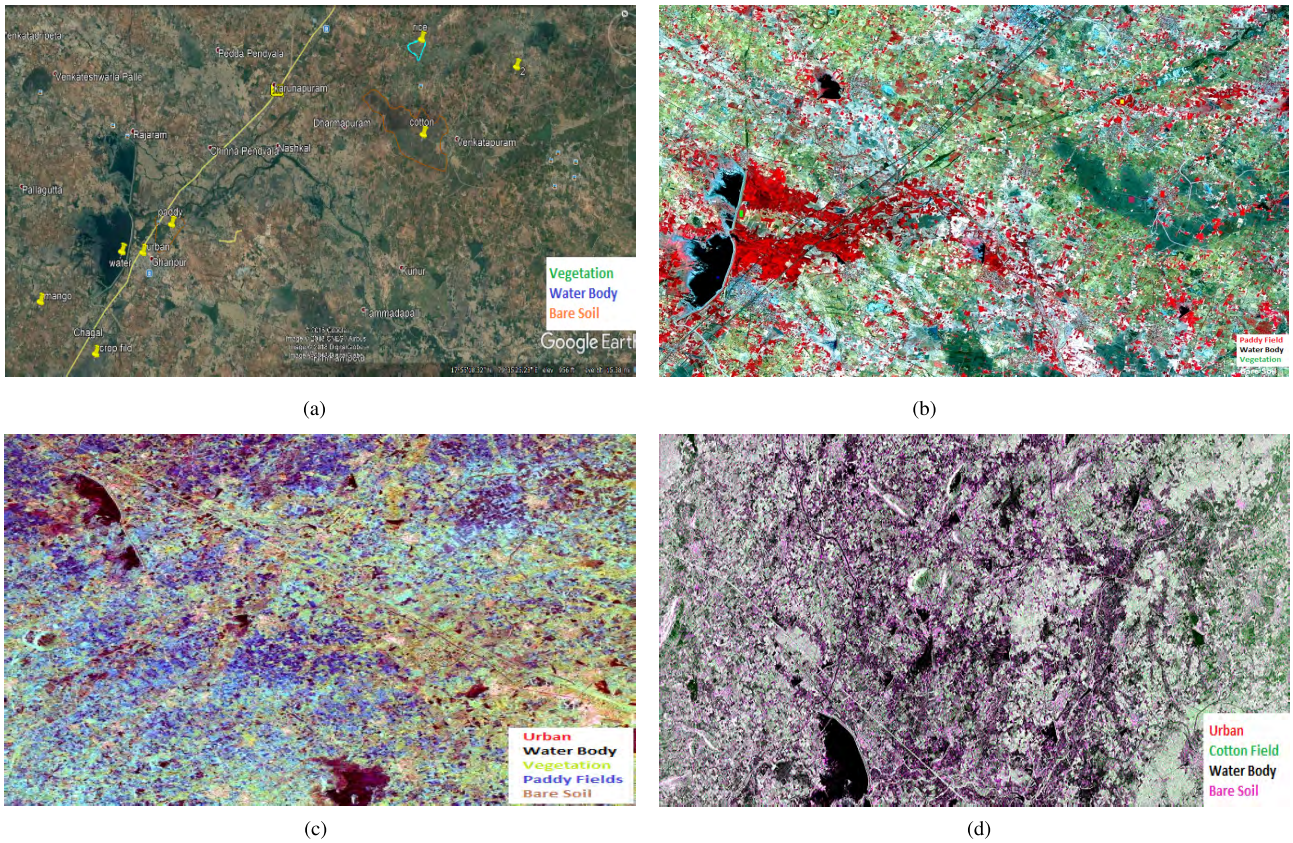

FIGURE 6. Images of Optical and Raney derived parameters of the Area of Interest. (a) Google Earths image. (b) Resourcesat-2 LISS- IV image. (c) Raney derived RGB image on hybrid pol data. (d) Raney derived RGB image on dual pol data.

IV. RESULTS AND DISCUSSION

To evaluate the results of SVM classifier, m-delta and m-chi decomposed images of RISAT-1, Resourcesat-2 and Google Earth images were used. The confusion matrix is used to assess the performance of the SVM classifier.

Fig. 6(a), is the Google Earth image, green color indicates vegetation, White Color indicates settlements, green color indicates water-bodies and brown color indicates bare soil. Fig 6(b), is the FCC image of LISS-IV data, where red color indicates paddy fields, black color indicates water body, green color indicates vegetation, and white color indicates bare soil. Fig 6(c), is the Raney derived RGB image on Hybrid pol data, where red color indicates urban settlements, black color indicates water body, green color indicates vegetation, and white color indicates bare soil. Fig 6(d), is the Raney derived RGB image on Dual pol data, where green color indicates vegetation, black color indicates water bodies and red color indicates urban settlements and paddy fields.

Fig. 7(a), is the Pseudo compact decomposition performed on Hybrid-pol data. From this decomposition, we obtain volume scattering, double bounce scattering and surface scattering. Where green color corresponds to the volume scattering from thick vegetation, red color corresponds to the surface scattering from crop fields and water bodies, blue color corresponds to the double bounce scattering from urban settlements. Fig. 7(b) and 7(c) are the m-delta and m-chi decomposed images, respectively. From m-delta and m-chi decompositions, yellow color corresponds to the double bounce from urban structures, i.e., buildings, green color corresponds to the volume scattering from vegetations. The magenta color corresponds to the surface scattering from crop fields, bare soil and dark blue corresponds to water bodies. It was observed visually that m-delta and m-chi decomposition results were almost similar. Fig. 7(d) and 7(e) are the SVM classified images on Hybrid-pol RISAT-1 data and Dual-pol RISAT-1 data, where red color corresponds to urban, green color corresponds to water body, blue color corresponds to vegetation and yellow color corresponds to bares soil. Fig. 7(e) is the SVM classified image on optical LISS-IV data, where blue color corresponds to water body, green color corresponds to vegetation, red color corresponds to bare soil, yellow color corresponds to urban.

The Table 4 represents the performance of kernel parameters for Land cover classification using SVM classifier. In this study, we have compared all kernel parameters (linear, polynomial, RBF) on the test data. In this paper, the method of SVM is implemented by using the library LIBSVM on Polsarpro tool. In this study, OAO approach has been retained with RBF kernel. The kernel parameters Cost Parameter (C) and kernel parameter (Gamma) are tuned

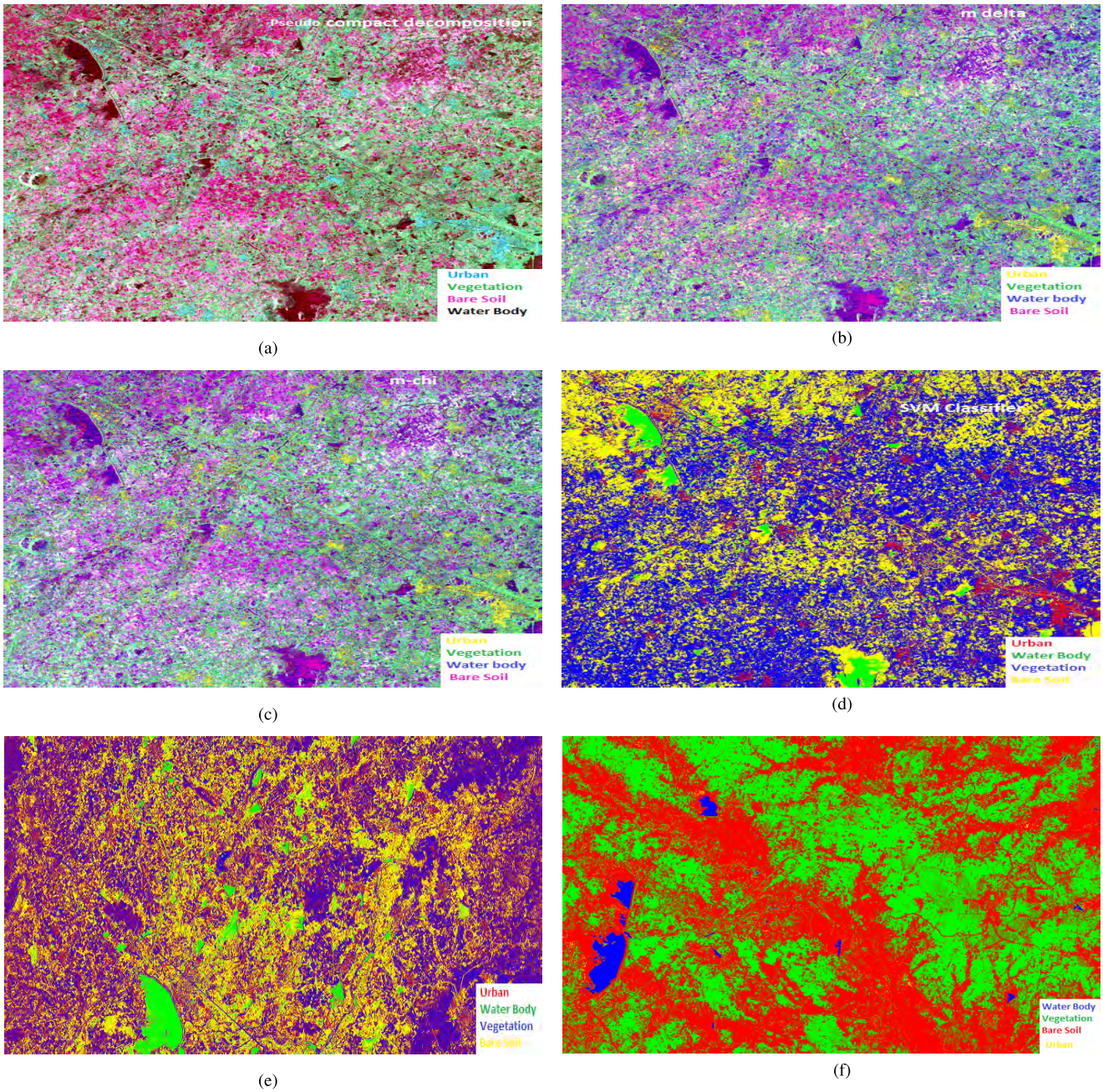

FIGURE 7. Results of Pseudo three component, m-delta, m-chi decompositions, SVM classification on RISAT-1 Hybrid pol data, dual pol data and optical LISS-IV data. (a) Psuedo compact decomposition. (b) m-Delta. (c) m-Chi. (d) SVM classified image on hybrid pol RISAT-1 data. (e) SVM classified image on dual pol RISAT-1 data. (f) SVM classification on LISS IV data.

in the range of C = (8,16,32,64,128,256) and gamma = (0.03,0.06,0.12,0.25,0.5,1,2). The cost parameter C and kernel parameter gamma were optimized using cross-validation for obtaining best possible classification accuracy [26]. From five-fold cross validation, we have obtained the values of C = 64, gamma = 0.5 with an accuracy 93.55% using grid search within a given set. While tuning the kernel parameters we have observed, as the values of C and gamma increases the accuracy also increases as shown in Fig. 9. With a large values of C and gamma, there is a tendency for the SVM to over-fit to the training data. The cross-validation procedure prevents the over-fitting problem. From the Table 4, we can conclude that RBF kernel parameter shows better Overall Accuracy (OA) of 92.36% when compared to Linear parameter 89.79 % and Polynomial parameter with degree '2' 88.44 %. The same number of training and test samples were applied to the individual classes for performing accuracy assessment for all kernel parameters. We also observe that urban class was better classified by RBF parameter than linear and polynomial parameters. The water body class, was well equally classified

TABLE 4. Accuracy assessment for various kernel parameters using confusion matrix for hybrid-pol RISAT-1 data.

	RBF				P '2'				L				CP
	U	WB	V	BS	U	WB	V	BS	U	WB	V	BS	
U	89.61	0.00	7.45	2.94	75.16	0.26	22.43	2.15	78.44	0.00	20.00	1.55	10097
WB	0.00	97.79	0.00	2.21	0.00	100	0.00	0.00	0.00	100	0.00	0.00	9582
V	6.11	0.47	73.97	19.45	3.64	0.32	86.41	9.63	4.34	0.18	85.95	9.53	1715
BS	0.00	1.12	3.45	95.42	0.00	0.17	0.17	99.39	0.00	0.17	0.35	99.48	2403
OA	92.36%				88.44%				89.79%				

RBF: Radial Basis Function; P '2': Polynomial; L: Linear U: Urban Class; WB: Water Body, V: Vegetation; BS: Bare Soil

TABLE 5. Confusion matrix for RISAT-1 (Hybrid-pol and Dual-pol) and optical LISS-IV data using SVM RBF kernel.

	RISAT-I Hybdrid Pol				RISAT-I Dual Pol				LISS-IV			
	U	WB	V	BS	U	WB	V	BS	U	WB	V	BS
U	89.61	0.00	7.45	2.94	56.66	0.00	35.32	8.02	86.69	0.01	0.00	45.08
WB	0.00	97.79	0.00	2.21	0.00	96.60	0.00	0.40	0.00	99.99	0.00	0.00
V	6.11	0.47	73.97	19.45	42.02	0.00	57.61	0.37	8.97	0.00	96.90	0.64
BS	0.00	1.12	3.45	95.42	2.89	2.58	1.07	93.46	4.34	0.17	0.06	54.28
OA	92.36%				76.83%				93.59%			

RBF: Radial Basis Function; P '2': Polynomial; L: Linear U: Urban Class; WB: Water Body, V: Vegetation; BS: Bare Soil

by all parameters. The vegetation class was better classified by polynomial parameter than linear and RBF parameters. The bare soil class was almost equally classified by all three parameters.The results of classification algorithm are evaluated using the Producer Accuracy (PA) and the User Accuracy (UA). The producer accuracy is defined as the ratio of pixels correctly classified to the number of pixels in that class. Similarly, UA is defined as the ratio of pixels correctly classified to the pixels labeled as this class. The Producer Accuracy of the classes urban, water-bodies, vegetation and bare soil are 0.98, 0.99, 0.60, 0.73 for RISAT-1 hybrid pol using RBF kernel. Similarly, the User Accuracy of the classes urban, water-bodies, vegetation and bare soil are 0.89, 0.97, 0.73, 0.95 for RISAT-1 hybrid pol using RBF kernel. The omission error of the classes urban, water-bodies, vegetation and bare soil are 10.39, 2.21, 26.03, 4.57. Similarly, the commission error of the classes urban, water-bodies, vegetation and bare soil are 1.14, 0.37, 39.69, 26.86.

The Table 5 represents the confusion matrix obtained for RISAT-1 Hybrid pol data, RISAT-1 Dual pol data and LISS-IV data using SVM classifier with RBF kernel parameter. We observe that (OA) 92.36% for Hybrid pol data is more when compared to Dual pol data 76.83%. We also observe that RISAT-1, Hybrid-pol data results and Optical LISS-IV results are almost similar.

From Table 6, it represents the training samples and test samples of the RISAT-1 hybrid pol data based on the inclusion of Ground Truth survey points. There was no overlap between the training and test data.

Fig. 8, shows the ground truth images of the given AOI on the date of acquisition with four classes. Fig. 8(a) shows buildings (urban) class, Fig. 8(b) shows water body class, Fig. 8(c) shows vegetation class, Fig. 8(d) shows the bare soil

TABLE 6. Training and test samples used for RISAT-1 Hybrid-Pol data classification.

Class	Training samples	Number of Polygons	Test samples	Number of Polygons
Urban	4699	02	10097	05
Water Body	3355	04	9582	08
Vegetation	5005	02	1715	09
Bare soil	1147	02	2403	03

class. Backscatter response from the urban area is considered as double-bounce scattering. Similarly, the response from water bodies and bare soil is considered as odd bounce scattering, and response from vegetation is considered as volume scattering. Fig. 8(e) shows the mango tree plantation which corresponds to the volume scattering. In order to understand the crop pattern, we need to take inputs from the local farmers regarding seasonal crop, duration of the crop, stages of the crop as shown in Fig. 8(f)-(h), respectively. It maybe observed that Fig. 8(e)-(h) corresponds to the vegetation class of various stages.

Table 7 shows the sigma naught values (RH, HH, RV, HV), degree of polarization values and relative phase values (in radians) for hybrid-pol and dual-pol datasets across various classes. From the Table 7, it has been observed that the sigma naught values for urban and vegetation are high due to double bounce and volume scattering and appears to be brighter due to strong returns. On the contrary, the sigma naught values for waterbodies and bare soil achieved are less due to specular reflection which is desirable. It is also observed that the DoP for urban is almost equal to 1 since it a pure target, whereas the other three target have less DoP values due to depolarization effect. Similarly, it can be observed that

FIGURE 8. Ground truth of various targets. (a) Urban. (b) Water body. (c) Vegetation. (d) Bare soil. (e) Mango plantation. (f) Paddy field (Stage-1). (g) Paddy field (Stage-2). (h) Paddy field (Stage-3).

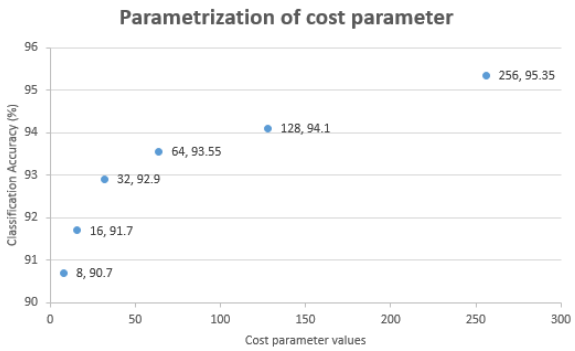

FIGURE 9. Parametrization of cost parameter.

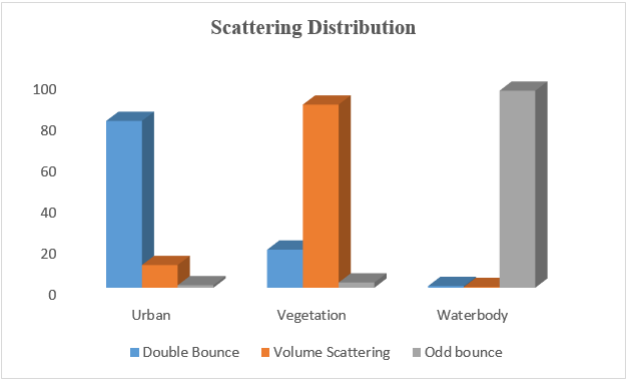

FIGURE 10. Scattering distribution of the targets over AOI.

TABLE 7. Sigma naught, DOP and relative phase values of dual and Hybrid pol RISAT-1 data.

Class	Sigma RH(dB)	Sigma HH(dB)	Sigma RV(dB)	Sigma HV(dB)	DoP (m)	Relative Phase(δ)
U	-7.761	-2.09	-8.247	-15.61	0.833	-1.133
WB	-20.698	-17.58	-18.331	-25.52	0.3124	2.2272
V	-10.821	-18.59	-8.4543	-16.52	0.6003	0.14
BS	-11.3143	-19.45	-13.1582	-10.72	0.2887	1.4769

the relative phase values for urban and vegetation are low and high for waterbodies and bare soil. The values from the Table 7 are the mean values taken from ten different locations of each class.

Fig. 10 shows the scattering distribution of the targets over AOI. It has been observed that the double bounce effect is predominant in urban class, whereas the volume scattering is low and the odd bounce is negligible. Moreover, the volume scattering is more dominant than double and odd bounce in vegetation class. The odd bounce effect is more dominant in water body, whereas the double bounce and volume scattering are negligible.

V. CONCLUSION

In hybrid polarimetry, to characterize the return signal, Stokes parameters are sufficient. Hybrid-pol (compact polarimetry) SAR is a new SAR mode, with a combination of wider swath along with coherent dual polarization with relative phase information. Therefore, Hybrid-pol (compact polarimetry) SAR is always the best choice when transmitted power and swath width are the main constraints. From this study,

using m-delta, m-chi decomposition, Raney decomposition and Pseudo Three Component decomposition techniques, we have characterized and classified various ground target classes in the data very well. The m-chi decomposition approach has been proven to be robust even though the transmitting signal is not perfectly circular polarized. This paper investigated the capability of m-delta and m-chi decomposition on various ground targets to understand their scattering response. SVM classifier has classified the dataset very well, and the results are very satisfactory. Few studies exclusively on Compact pol data are reported only to (80-85)% Overall Accuracy (OA) [33]–[36]. In this study, we have obtained (OA) of 92.36% for hybrid Pol RISAT-1 data using OAO algorithm with kernel parameters $C = 64$ and gamma $= 0.5$. Similarly, SVM with RBF kernel parameter gave an Overall Accuracy (OA) of 76.83% for dual-pol RISAT-1. Achieving good OA on Hybrid pol data is because of the sound knowledge of the Ground Truth data and also in giving training sites to the classifier. We have observed in SVM classification that a polynomial kernel takes longer time when compare to RBF kernel. Thus from this study, we can conclude that Hybrid pol data is always preferred over Dual pol data with respective to information content. The preprocessing and classification were performed using PolSARpro, Envi SARscape, and SARc view. The results are verified with optical imagery of Resourcesat-2, LISS IV data, Google Earth and In-situ data.

ACKNOWLEDGMENT

The authors would like to thank the NRSC Data Center (NDC) Hyderabad for providing the datasets for this study, the European Space Agency (ESA) for providing PolSARpro, a SAR Processing Tool for this study, and the faculty, Prof. Y. S. Rao and scholars of CSRE Department, IIT Bombay for assisting in this study. They would like to dedicate this work to our beloved Prof. Late Wolfgang-Martin Boerner. They would also like to thank the anonymous reviewers for their valuable constructive comments which improved the quality and readability of this paper.

REFERENCES

[1] *Bhaskara—I Mission*. Accessed: Aug. 3, 2017. [Online]. Available: http://www.isro.gov.in/Spacecraft/bhaskara-i

[2] *List of Spacecraft*. Accessed: Aug. 3, 2017. [Online]. Available: http://www.isro.gov.in/list-of-spacecrafts

[3] *Earth Observation Missions*. Accessed: Aug. 3, 2017. [Online]. Available: https://www.nrsc.gov.in/Remote_Sensing_Data_Policy?q=Earth_Observation_Missions

[4] *Annual Report*. Accessed: Aug. 3, 2017. [Online]. Available: http://www.isro.gov.in/sites/default/files/AnnualRepo-rts/2014/EOS.html

[5] *RISAT-2 Handbook*. Accessed: Jul. 2, 2016. [Online]. Available: https://www.nrsc.gov.in/Remote_Sensing_Data_Polic-y?q=RISAT-2

[6] *RISAT-1 Handbook*. Accessed: Jul. 2, 2016. [Online]. Available: https://nrsc.gov.in/uim_2014_proceedings/infolets/RI-SAT1_Handbook.pdf

[7] J. N. Goswami and M. Annadurai, "Chandrayaan-1: India's first planetary science mission to the moon," *Current Sci.*, vol. 96, no. 4, pp. 486–491, 2009.

[8] R. K. Raney *et al.*, "The lunar mini-RF radars: Hybrid polarimetric architecture and initial results," *Proc. IEEE*, vol. 99, no. 5, pp. 808–823, May 2011.

[9] F. J. Charbonneau *et al.*, "Compact polarimetry overview and applications assessment," *Can. J. Remote Sens.*, vol. 36, pp. S298–S315, Jun. 2010.

[10] J. A. Richards, *Remote Sensing With Imaging Radar*. Berlin, Germany: Springer, 2009, pp. 53–106.

[11] R. K. panigrahi and A. K. Mishra, "Comparison of hybrid-Pol with quad-Pol scheme based on polarimetric information content," *Int. J. Remote Sens.*, vol. 33, no. 11, pp. 3531–3541, 2012.

[12] J.-C. Souyris, P. Imbo, R. Fjortoft, S. Mingot, and J.-S. Lee, "Compact polarimetry based on symmetric properties of geophysical media: The $\pi/4$ mode," *IEEE Trans. Geosci. Remote Sens.*, vol. 43, no. 3, pp. 634–645, Mar. 2005.

[13] J. C. Souyris and S. Mingot, "Polarimetry based on one transmitting and two receiving polarizations: The $\pi/4$ mode," in *Proc. Int. Geosci. Remote Sens. Symp. (IGARSS)*, 2002, pp. 629–631.

[14] M. E. Nord, T. L. Ainsworth, J. S. Lee, and N. J. S. Stacy, "Comparison of compact polarimetric synthetic aperture radar modes," *IEEE Trans. Geosci. Remote Sens.*, vol. 47, no. 1, pp. 174–188, Jan. 2009.

[15] R. Touzi, "Compact-hybrid versus linear-dual and fully polarimetric SAR," in *Proc. 4th Int. Workshop Sci. Appl. SAR Polarimetry Polarimetric Interferometry (PolInSAR)*, 2009. [Online]. Available: https://earth.esa.int/documents/10174/1597298/SAR68

[16] R. K. Raney, "Hybrid-polarity SAR architecture," *IEEE Trans. Geosci. Remote Sens.*, vol. 45, no. 11, pp. 3397–3404, Nov. 2007.

[17] M. Chakraborty *et al.*, "Initial results using RISAT-1 C-band SAR data," *Current Sci.*, vol. 104, no. 4, pp. 490–501, 2013.

[18] *Resourcesat-2 Handbook*. Accessed: Jul. 2, 2016. [Online]. Available: https://nrsc.gov.in/uim_2014_proceedings/infolets/Res-ourcesat2_Handbook.pdf

[19] R. K. Raney, "Dual-polarized SAR and Stokes parameters," *IEEE Geosci. Remote Sens. Lett.*, vol. 3, no. 3, pp. 317–319, Jul. 2006.

[20] S. R. Cloude, D. G. Goodenough, and H. Chen, "Compact decomposition theory," *IEEE Geosci. Remote Sens. Lett.*, vol. 9, no. 1, pp. 28–32, Jan. 2012.

[21] R. K. Raney, J. T. S. Cahill, G. W. Patterson, and D. B. J. Bussey, "The m-chi decomposition of hybrid dual-polarimetric radar data," in *Proc. Int. Geosci. Remote Sens. Symp. (IGARSS)*, 2012, pp. 5093–5096.

[22] V. Turkar and Y. S. Rao, "Classification of polarimetric synthetic aperture radar images from SIR-C and ALOS PALSAR," in *Proc. Int. Conf. Recent Adv. Microw. Theory Appl. (MICROWAVE)*, Nov. 2008, pp. 438–440.

[23] G. Mountrakis, J. Im, and C. Ogole, "Support vector machines in remote sensing: A review," *ISPRS J. Photogram. Remote Sens.*, vol. 66, no. 3, pp. 247–259, 2011.

[24] V. N. Vapnik, "An overview of statistical learning theory," *IEEE Trans. Neural Netw.*, vol. 10, no. 5, pp. 988–999, Sep. 1999.

[25] C. Cortes and V. Vapnik, "Support-vector networks," *Mach. Learn.*, vol. 20, no. 3, pp. 273–297, 1995.

[26] *A Practical Guide to Support Vector Classification*. Accessed: Apr. 4, 2018. [Online]. Available: https://www.csie.ntu.edu.tw/~cjlin/papers/libsvm.pdf

[27] P. Mishra, D. Singh, and Y. Yamaguchi, "Land cover classification of PALSAR images by knowledge based decision tree classifier and supervised classifiers based on SAR observables," *Prog. Electromagn. Res.*, vol. 30, pp. 47–70, 2011.

[28] B. H. Trisasongko, D. R. Panuju, D. J. Paull, X. Jia, and A. L. Griffin, "Comparing six pixel-wise classifiers for tropical rural land cover mapping using four forms of fully polarimetric SAR data," *Int. J. Remote Sens.*, vol. 38, no. 11, pp. 3274–3293, 2017.

[29] C. Lardeux *et al.*, "Support vector machine for multifrequency SAR polarimetric data classification," *IEEE Trans. Geosci. Remote Sens.*, vol. 47, no. 12, pp. 4143–4152, Dec. 2009.

[30] C. J. C. Burges, "A tutorial on support vector machines for pattern recognition," *Data Mining Knowl. Discovery*, vol. 2, no. 2, pp. 121–167, 1998.

[31] B. Yekkehkhany, A. Safari, S. Homayouni, and M. Hasanlou, "A comparison study of different kernel functions for SVM-based classification of multi-temporal polarimetry SAR data," *Int. Arch. Photogram., Remote Sens. Spatial Inf. Sci.*, vol. 40, no. 2, p. 281, 2014.

[32] B. Souissi, M. Ouarzeddine, and A. Belhadj-Aissa, "Optimal SVM classification for compact polarimetric data using Stokes parameters," *J. Math. Model. Algorithms Oper. Res.*, vol. 13, no. 4, pp. 433–446, 2014.

[33] D. Haldar, A. Das, S. Mohan, O. Pal, R. S. Hooda, and M. Chakraborty, "Assessment of L-band SAR data at different polarization combinations for crop and other landuse classification," *Prog. Electromagn. Res.*, vol. 36, pp. 303–321, 2012.
[34] V. Turkar, S. De, Y. S. Rao, S. Shitole, A. Bhattacharya, and A. Das, "Comparative analysis of classification accuracy for RISAT-1 compact polarimetric data for various land-covers," in *Proc. Int. Geosci. Remote Sens. Symp. (IGARSS)*, 2013, pp. 3586–3589.
[35] H. Padalia and S. Yadav, "Evaluation of RISAT-1 SAR data for tropical forestry applications," *Adv. Space Res.*, vol. 59, no. 1, pp. 2–11, 2017.
[36] B. Mishra and J. Susaki, "Land cover classification comparisons among dual polarimetric, pseudo-fully polarimetric, and fully polarimetric SAR imagery," *Proc. SPIE* vol. 8524, p. 852408, Nov. 2012. [Online]. Available: https://spie.org/Publications/Proceedings/Volume/8524?&origin_id=x4318&event_id=985293

KIRAN DASARI (S'15) was born in Hyderabad, India, in 1989. He received the B.Tech. degree in ECE and the M.Tech. degree in Embedded Systems (ECE) from JNTU Hyderabad in 2010 and 2012, respectively. He is currently pursuing the Ph.D. degree from the National Institute of Technology, Warangal, India. His field of study is microwave imaging, radar polarimetry, compact polarimetry, and other areas of interest are radar signal processing, remote sensing. He is a member of the IEEE Geoscience and Remote Sensing Society since 2018 and the IEICE, Japan.

ANJANEYULU LOKAM (M'10) was born in 1967 in India. He received the B.Tech. (ECE), M.Tech. degree, and Ph.D. degrees from the National Institute of Technology (NIT), Warangal, India in 1989, 1991, and 2010, respectively. He was the Project Officer at the Institute of Armament Technology, Pune, India, for five years since 1991, and was involved in the design of surface borne and air-borne radar systems for clutter measurement application. He worked as a Staff Scientist at Helios Systems, Chennai, India, for two years, and was involved in the development of radio wave propagation assessment software modules for ship-borne radars. He has been with the Department of Electronics and Communications Engineering, NIT, Warangal, India, since 1997. His areas of interest include computer networks, electromagnetic field theory, microwave & radar engineering, microwave remote sensing, radar polarimetry, hybrid polarimetry, and neural networks & fuzzy logic systems. He has completed few defence R&D Projects and has 50 papers to his credit in national and international conferences and journals. He is a Fellow of Institution of Engineers, a Life Member of ISTE, and a member of the IEEE Antennas and Propagation Society and the IEEE Signal Processing Society since 2010.